International Journal of Nanomedicine

Dovepress
open access to scientific and medical research

Open Access Full Text Article

ORIGINAL RESEARCH

Multifunctional Nanoparticles Codelivering Doxorubicin and Amorphous Calcium Carbonate Preloaded with Indocyanine Green for Enhanced Chemo-Photothermal Cancer Therapy

Jingmou Yu[1–3], Liangliang Wang[4], Xin Xie[2], Wenjing Zhu[3], Zhineng Lei[3], Linghui Lv[3], Hongling Yu[3], Jing Xu[4], Jin Ren[2,3]

[1]Huzhou Key Laboratory of Medical and Environmental Applications Technologies, School of Life Sciences, Huzhou University, Huzhou, People's Republic of China; [2]Jiangxi Provincial Laboratory Laboratory of System Biomedicine, Jiujiang University, Jiujiang, People's Republic of China; [3]School of Pharmacy and Life Sciences, Jiujiang University, Jiujiang, People's Republic of China; [4]Affiliated Hospital of Jiujiang University, Jiujiang, People's Republic of China

Correspondence: Jingmou Yu; Jin Ren, Email yjm1016@hotmail.com; yanjiushengrj@126.com

Background: Multifunctional stimuli-responsive nanoparticles with photothermal-chemotherapy provided a powerful tool for improving the accuracy and efficiency in the treatment of malignant tumors.

Methods: Herein, photosensitizer indocyanine green (ICG)-loaded amorphous calcium-carbonate (ICG@) nanoparticle was prepared by a gas diffusion reaction. Doxorubicin (DOX) and ICG@ were simultaneously encapsulated into poly(lactic-co-glycolic acid)-ss-chondroitin sulfate A (PSC) nanoparticles by a film hydration method. The obtained PSC/ICG@+DOX hybrid nanoparticles were characterized and evaluated by Fourier transform infrared spectroscopy (FTIR), dynamic light scattering (DLS), transmission electron microscopy (TEM), and differential scanning calorimetry (DSC). The cellular uptake and cytotoxicity of PSC/ICG@+DOX nanoparticles were analyzed by confocal laser scanning microscopy (CLSM) and MTT assay in 4T1 cells. In vivo antitumor activity of the nanoparticles was evaluated in 4T1-bearing Balb/c mice.

Results: PSC/ICG@+DOX nanoparticles were nearly spherical in shape by TEM observation, and the diameter was 407 nm determined by DLS. Owing to calcium carbonate and disulfide bond linked copolymer, PSC/ICG@+DOX nanoparticles exhibited pH and reduction-sensitive drug release. Further, PSC/ICG@+DOX nanoparticles showed an effective photothermal effect under near-infrared (NIR) laser irradiation, and improved cellular uptake and cytotoxicity in breast cancer 4T1 cells. Importantly, PSC/ICG@+DOX nanoparticles demonstrated the most effective suppression of tumor growth in orthotopic 4T1-bearing mice among the treatment groups. In contrast with single chemotherapy or photothermal therapy, chemo-photothermal treatment by PSC/ICG@+DOX nanoparticles synergistically inhibited the growth of 4T1 cells.

Conclusion: This study demonstrated that PSC/ICG@+DOX nanoparticles with active targeting and stimuli-sensitivity would be a promising strategy to enhance chemo-photothermal cancer therapy.

Keywords: chemo-photothermal treatment, amorphous calcium carbonate, nanoparticles, stimuli-sensitivity, drug delivery, cancer therapy

Introduction

Calcium carbonate ($CaCO_3$), a nontoxic biomineral, was used as a potential carrier in biomedical applications, owing to its intrinsic advantages of degradability at acid pH conditions, biocompatibility, and easy production.[1–3] Especially, amorphous calcium carbonate (ACC) could be readily prepared in a nanoscaled size.[4,5] Some researchers have employed monodispersed ACC nanoparticles as a template to construct a drug-preloaded system.[6] However, ACC is insoluble in water and capable to release its payload in acid media. These obstacles limited its wide application in the medical field.

Received: 26 October 2022
Accepted: 7 January 2023
Published: 18 January 2023

Graphical Abstract

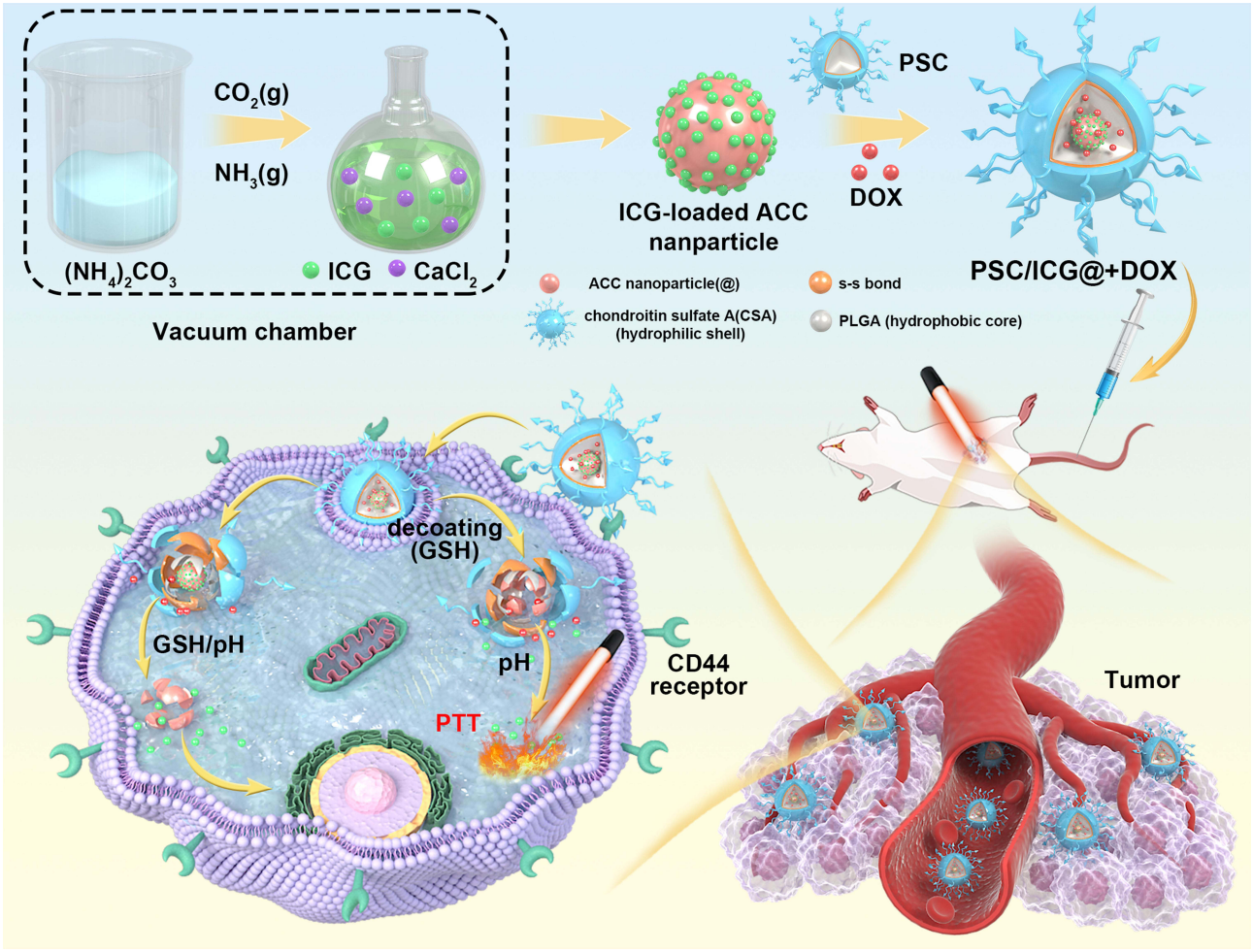

To address the issue, hybrid nanoparticles have been fabricated to improve the stability of ACC nanoparticles and drug bioavailability.[7] Liu et al developed phospholipid and $CaCO_3$ hybrid nanoparticles, which were coated with phospholipid and polyethylene glycol, leading to isolate the ACC nanoparticles from an aqueous medium.[8]

In recent years, the amphiphilic copolymer has been utilized as a drug carrier, which is composed of hydrophilic and hydrophobic groups.[9,10] It can be self-assembled nanoparticles in an aqueous medium and form core-shell architecture. The inner core could encapsulate the hydrophobic antitumor drugs. These nanoparticles exhibit excellent characteristics, such as improved solubility of insoluble drugs and enrichment in tumor sites via enhanced permeation and retention (EPR) effect.[11] Inspired by the typical core-shell structure, we envisaged that polymeric nanoparticles with inner reservoirs were introduced for the protection of ACC. This system consists of a core with drug-preloaded ACC and a shell of polymeric coatings. In order to effectively control drug release, the shell materials should be degradable. Microenvironment-responsive nanocarrier provided a new approach, which could be disintegrated and accelerate drug release in response to certain stimuli,[12] particularly to intracellular low pH and high concentration of reduced glutathione (GSH).[13,14] Among these nanocarriers, redox-sensitive nanoparticles have received more attention for the triggered release of anticancer drug molecules in tumor sites.[15,16] Disulfide bonds could be highly stable in the extracellular milieu, while quickly disrupted by high GSH via thiol-disulfide exchange reaction in the cytoplasm of tumor cells.[17,18] Our

groups have synthesized reduction-sensitive PSC conjugate,[19] and DOX-containing PSC nanoparticles showed reduction-sensitive drug release behavior and enhanced the cytotoxicity of DOX against A549 cells.

Polymeric nanoparticles were usually applied for the delivery of a single chemotherapy agent.[20,21] Current cancer therapy has gradually changed from single therapy into combinational therapy, such as photothermal therapy (PTT), photodynamic therapy, immunotherapy and gene therapy.[22–24] It integrated the merits of various treatments. PTT utilizes photosensitizing agents to generate thermal energy, leading to the ablation of tumor cells.[25] This treatment has the advantages of non-invasiveness and safety. Indocyanine green (ICG) is a kind of near-infrared (NIR) absorbing dyes,[26,27] and is also an effective photosensitive drug for PTT.[28,29] However, free ICG cannot selectively distribute in tumor sites and exhibit a short half-life time.[30] It limited its wide application in medical fields.

In the present work, the aim is to design multifunctional nanoparticles as drug carriers for chemo-PTT tumor therapy. First, ICG was pre-loaded into amorphous calcium-carbonate (ICG@) nanoparticles. PSC polymeric nanoparticles entrapped both DOX and ICG@. The final PSC/ICG@+DOX nanoparticles were obtained and evaluated. In vitro drug release and cellular evaluation of PSC/ICG@+DOX nanoparticles were performed. Furthermore, in vivo tumor growth inhibition of the nanoparticles was carried out in orthotopic 4T1-bearing Balb/c mice.

Materials and Methods

Materials

Calcium chloride dihydrate and ammonium carbonate were provided by Sinopharm Chemical Reagent Co., Ltd (Shanghai, China). Cystamine dihydrochloride was purchased from Alfa Aesar Chemical Co., Ltd (Shanghai, China). Chondroitin sulfate A was obtained from Tokyo Chemical Industry Co., Ltd. (Tokyo, Japan). Poly(lactic-co-glycolic acid) (PLGA, 20 kDa) was provided by Jinan Daigang Biomaterial Co., Ltd. (Jinan, China). ICG, Doxorubicin (DOX), GSH, Hoechst 33342, *N*-(3-dimethylaminopropyl)-*N'*-ethylcarbodiimide hydrochloride (EDC) and 3-(4, 5-dimethyl-2-thiazolyl)-2,5-diphenyltetrazolium bromide (MTT) were purchased from Shanghai Aladdin Bio-Chem Technology Co., Ltd. (Shanghai, China). Doxorubicin hydrochloride (DOX·HCl) was provided by Beijing Huafeng United Technology Co, Ltd. (Beijing, China). RPMI 1640 medium and trypsin-EDTA were obtained from Zhejiang Ruisen Biotechnology Co., Ltd (Huzhou, China). Fetal bovine serum was provided by Zhejiang Tianhang Biotechnology Co., Ltd (Huzhou, China).

4T1 breast cancer cells were obtained from China Center for Type Culture Collection (Wuhan, China). The cells were cultured in RPMI-1640 media with the addition of 10% fetal bovine serum and 1% penicillin-streptomycin. The culture condition was in an atmosphere containing 5% CO_2 at 37°C. Female Balb/c mice and Kunming mice (4–6 weeks age) were provided by Hunan SLAC Jingda Laboratory Animal Co., Ltd (Changsha, China). All animal studies were approved by the Experimental Ethics Committee of Jiujiang University (Approval No. 2021-YX-015). All animal experiments followed the guidelines for Ethical Review of Laboratory Animal Welfare in China (GB/T35892-2018). The breeding conditions of laboratory animals were conducted in accordance with the requirements of environment and housing facilities in China (GB 14925-2010).

Preparation of ICG@ Nanoparticles

ACC nanoparticles were prepared by a gas diffusion reaction. In brief, $CaCl_2$ (1.0 g) was dissolved in 50 mL absolute ethanol. The solution was transferred into a flask, which was covered with aluminum foil and punctured with five pores. Then the flask and 66.5 mg $(NH_4)_2CO_3$ in a beaker were kept in a vacuum desiccator at 25°C. After 18 h reaction, ACC was collected by ultracentrifugation and rinsed with absolute ethanol. Subsequently, the ACC product was dried in a vacuum at room temperature. ICG@ nanoparticles were prepared in the same way except that 3.5 mg ICG was added into the ethanol solution containing CaCl2.

Preparation of PSC/ICG@+DOX Nanoparticles

PSC conjugate was first synthesized.[19] In brief, 500mg PLGA and 25 mg EDC were dispersed in 26 mL dimethyl sulfoxide (DMSO). Cystamine dihydrochloride (17 mg) was added under magnetic stirring. After 24 h, the mixture was dialyzed (MWCO: 14 kDa) against deionized water. Further, the dialysis solution was freeze-dried. Subsequently, the

obtained cystamine-modified PLGA (500 mg) was dispersed in DMSO and deionized water. Chondroitin sulfate A (720 mg) and EDC (24 mg) were dispersed in deionized water (18.7 mL) and DMSO (125 mL), and introduced into the above solution. After stirring for 24 h, this solution was dialyzed and freeze-dried. Then, PSC copolymer was obtained.

Secondly, PSC (25 mg) was dispersed in 10 mL of mixed solution (water: acetone=1:4, v/v). ICG@ (25 mg) was re-dispersed in 100 mL of anhydrous ethanol. Then, DOX (5 mg) in 5 mL acetone was gently dropped into ICG@ suspension under stirring. Next, the PSC nanoparticles were slowly introduced into the above solution. After 6 h, the solution was transferred to rotary-vacuum evaporation and followed by vacuum drying. A dried film was formed and dissolved into 20 mL of distilled water under stirring followed by probe ultrasonication. The nanoparticle suspensions were transferred into a dialysis bag against water. Finally, the dialysis solution was lyophilized and the obtained PSC/ICG@+DOX product was stored at 4°C. In the same way, PSC/ICG@ nanoparticles were prepared without the addition of DOX.

Characterization of PSC/ICG@+DOX Nanoparticles

The preparation of drug-containing nanoparticles was confirmed by FTIR (Bruker Tensor II, Germany). The drug state in the nanoparticles was measured by DSC (STA 8000, PerkinElmer, USA). The scanned temperatures were from 30°C to 300°C. The heating rate was 10°C/min. ACC or ICG@ nanoparticles were dispersed in anhydrous ethanol, while PSC/ICG@+DOX or PSC/ICG@ nanoparticles were in the aqueous medium. The particle distribution and zeta potentials of different nanoparticles were investigated by a zeta and laser sizer (90Plus, Brookhaven Instruments Corp., USA). The shape of the nanoparticles was detected by TEM (JEM-1230, Jeol, Japan) at 80 kV.

The amounts of DOX or ICG in the nanoparticles were investigated by ultraviolet–visible spectrophotometer. The detected wavelengths of DOX or ICG were set at 480 or 784 nm, respectively. The loading contents (LC) were calculated from the weight of encapsulating drug (DOX or ICG) divided by the amount of total drug-containing nanoparticles.[31]

Free ICG, PSC/ICG@ or PSC/ICG@+DOX dispersed in water were irradiated using a semiconductor laser device (Changchun Leishi Photo-Electric Technology Co., Ltd., China) for 5 min at 808 nm (2.2 W/cm^2). The final ICG concentration was 10 μg/mL. The temperature changes were detected by a thermocouple. Further, the thermal images were observed by an infrared imaging camera (Hikvision, H10, Hangzhou, China). The stability of ICG or ICG-loaded nanoparticles in aqueous media was further examined by quantifying the absorption value at 784 nm. The absorbance values were detected at scheduled time intervals.

In vitro Drug Release

In vitro drug release rates from drug-containing nanoparticles were investigated by a dialysis method. The sample solution (1 mL) was placed in a dialysis bag (MWCO: 14 kDa) and transferred into a tube with 20 mL release media at 37°C. In order to imitate the body condition, the media solutions were phosphate buffer solution (PBS, pH 7.4, with or without 20 mM GSH), or PBS (pH 5.5, with or without 20 mM GSH). The tubes were fixed in an air-bath shaker at 160 rpm. At scheduled time intervals, the media were replaced by 20 mL of fresh media. The concentration of DOX released was analyzed by a fluorescence spectrophotometer (Hitachi F-7000, Japan).[15]

In vitro Cellular Uptake

4T1 cells (1.0×10^5) were seeded into a glass-bottom culture dish with a diameter of 35 mm. After the cells were attached to the dish, the culture medium was discarded. Then the cells were treated with DOX·HCl, DOX·HCl+ICG, or PSC/ICG@+DOX nanoparticle. The equivalent concentrations of DOX and ICG were made at 5.3 and 2.0 μg/mL, respectively. After 4 h, the drug-containing media were removed and fresh media were added. Some cells were irradiated by an 808 nm laser (2.0 W/cm^2, 3 min). After 1 h incubation, the cells were washed with ice-cold PBS three times. Further, Hoechst 33342 (5 μg/mL) was added for 0.5 h in nuclei staining. The cells were fixed by 4% paraformaldehyde for another 0.5 h. Finally, the sample images were measured by confocal laser scanning microscope (CLSM, Leica SP8, Germany).

In vitro Cytotoxicity

In vitro inhibition efficacy of PSC/ICG@+DOX nanoparticles against 4T1 cells under NIR laser irradiation was assessed by the MTT method. Typically, 4T1 cells were seeded at 6000 cells/well in 96-well plates (Costar, Corning, NY, USA). As the cells adhered to the well, the media was removed. 150 μL of cultured media were added, in which DOX·HCl, free ICG, DOX·HCl+ICG, PSC/ICG@ and PSC/ICG@+DOX nanoparticles were diluted to various concentrations. After 18 h, the media were discarded and fresh culture media were added. Some cells were illuminated by an 808 nm laser (2 W/cm^2) for 3 min, and further incubated for 6 h. Then the medium was thrown away. 150 μL of MTT solution (500 μg/mL) was introduced and incubated for 4 h. Subsequently, the media were replaced by 150 μL DMSO. After 15 min, the absorbance value was detected at 490 nm by a microplate reader (Bio-Rad Laboratories, Inc., USA).

Biocompatibility Preliminary Evaluation

To assess the biocompatibility of the nanoparticles, female Kunming mice were randomly divided into 4 groups (n = 10): 1) 5% glucose; 2) PSC (50 mg/kg); 3) PSC/ICG@ (50 mg/kg); 4) PSC/ICG@+DOX (50 mg/kg). All mice received four doses on days 0, 3, 6 and 9 via tail vein injection. The body weight was measured every day. The experiment ended on day 10. The blood specimens were collected. Red blood cells (RBC), white blood cells (WBC), platelets, total bilirubin, blood urea nitrogen (BUN), creatinine levels, aspartate transaminase (AST) and alanine transaminase (ALT) were analyzed.[32]

In vivo Antitumor Effects

4T1 cells (2×10^6/mouse) were subcutaneously injected into the mammary fat pad of female Balb/c mice to establish tumor-bearing mice model.[33] The mice can be used for the following experiments as the tumor volumes reached approximately 150 mm^3. Nine groups of 4T1 tumor-bearing mice were randomly separated (n = 5). The administrations were as follows: 1) 5% glucose; 2) PSC (46.7 mg/kg, approximately equivalent to the content of polymers in PSC/ICG@+DOX nanoparticles); 3) DOX·HCl (3.2 mg/kg); 4) ICG (1.2 mg/kg), plus NIR irradiation; 5) DOX·HCl+ICG (1.2 mg/kg ICG, 3.2 mg/kg DOX), plus NIR irradiation; 6) PSC/ICG@ (1.2 mg/kg ICG); 7) PSC/ICG@ (1.2 mg/kg ICG), plus NIR irradiation; 8) PSC/ICG@+DOX (1.2 mg/kg ICG, 3.2 mg/kg DOX); 9) PSC/ICG@+DOX (1.2 mg/kg ICG, 3.2 mg/kg DOX), plus NIR irradiation. The administration was via tail vein injection every 3 days for 4 times. Each NIR irradiation at the tumor point was applied at 24 h after drug injection. An 808 nm laser was illuminated at 2.0 W/cm^2 for 5 min. The first day of intravenous injection was named day 0. The body weight and tumor volume were measured. The tumor volumes were calculated by the formula: 0.5 × length × $width^2$. After the 14th day, the mice were sacrificed. The tumor tissues were excised and fixed in 4% formalin. The tumor slices were subjected to hematoxylin and eosin (H&E), TdT-mediated dUTP nick end labeling (TUNEL) and Ki-67 analysis. The images were recorded by an optical microscope.

Statistical Analysis

Data were expressed as mean ± standard deviation. Statistical analysis was performed by one-way ANOVA. The difference $P < 0.05$ was considered significant, and $P < 0.01$ for highly significant.

Results and Discussion

Preparation and Characterization of PSC/ICG@+DOX Nanoparticles

The PSC/ICG@+DOX hybrid nanoparticles were fabricated by the synthesis of ICG@ and PSC conjugate, and the preparation of drug-containing nanoparticles. ICG@ was first synthesized by a vapor-diffusion method. Amphiphilic PSC nanoparticles were used to encapsulate ICG@ nanoparticles and DOX. The resultant nanoparticles were expected to increase the stability of ACC-based nanoparticles in aqueous media, and exhibit dually pH/GSH-responsive drug release behavior in the tumor microenvironment. The preparation of PSC/ICG@+DOX was verified by FTIR. As shown in Figure 1, ACC nanoparticles exhibited characteristic absorption peaks at 702, 869, and 1426 cm^{-1} (CO_3^{2-} bending vibration).[34] The low-intensity peak at 1633 cm^{-1} was ascribed to the bending vibration of strongly adsorbed water. Compared with ACC, ICG@ appeared new peaks at 1084 and 1466 cm^{-1}, and exhibited a stronger peak at 1426 cm^{-1}. It verified that ICG had been loaded into ACC nanoparticles. As displayed in Figure 1D, the peaks of amide bands I and II

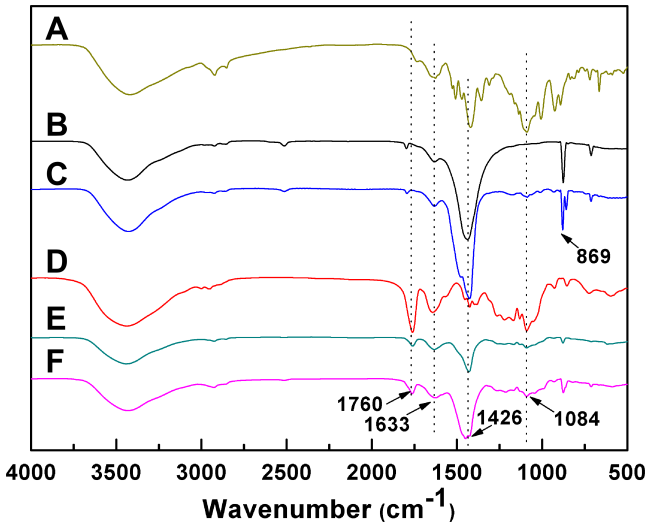

Figure 1 FTIR patterns of (**A**) ICG, (**B**) ACC, (**C**) ICG@, (**D**) PSC, (**E**) PSC/ICG@ and (**F**) PSC/ICG@+DOX nanoparticles.

in PSC conjugate were seen at 1633 and 1760 cm^{-1}. In contrast with PSC, the peaks of PSC/ICG@ at 1426 cm^{-1} significantly increased, which belonged to the peak of ICG@. This result indicated that the ICG@ was effectively loaded into PSC nanoparticles. Furthermore, the peaks at 869 and 1084 cm^{-1} increased in PSC/ICG@+DOX. Therefore, the hybrid PSC/ICG@+DOX nanoparticles were successfully prepared.

DSC was adopted to analyze the thermal behavior of the drug in the nanoparticles. As presented in Figure S1 (Supporting Information), DOX and ICG exhibited melting points at 194°C and 241°C, respectively. Since the melting point for different polymorphs of $CaCO_3$ ranged from 825°C to 1339°C.[34] ICG@ nanoparticles did not exhibit an obvious peak up to 300°C. Furthermore, no endothermic peaks were detected for PSC/ICG@ and PSC/ICG@+DOX. These results demonstrated that DOX and ICG were in an amorphous state in drug-containing nanoparticles.

As shown in Figures 2A and B, ACC and ICG@ nanoparticles were amorphous in shape. Due to the dried state of the sample, TEM images of ACC and ICG@ nanoparticles were aggregated. The particle size of ICG@ dispersed in ethanol was 221 nm by DLS, which was larger than that of ACC at 123 nm (Table 1). This indicated that ICG was incorporated into ACC nanoparticles. The ICG content in ICG@ was 12.43%. The zeta potentials of ACC and ICG@ were 20.99 and 30.34 mv, respectively.

PSC/ICG@+DOX nanoparticles were prepared by a film hydration method. PSC conjugate was composed of PLGA and chondroitin sulfate A with disulfide bond linkage, and exhibited biodegradability and reduction sensitivity.[19] As shown in Table 1, ICG and DOX loading contents in PSC/ICG@+DOX nanoparticles were 2.57% and 6.79%, respectively. Similarly, PSC/ICG@ nanoparticles were obtained by using the same method. The size of PSC/ICG@ nanoparticles was 335 nm by DLS. In addition, the diameter of PSC/ICG@ was larger than that of ICG@. This is due to the coating and space occupation by PSC nanoparticles. Further, the diameter of PSC/ICG@ was smaller than that of PSC/ICG@+DOX. It was due to DOX encapsulation in PSC/ICG@+DOX nanoparticles. As shown in Figures 2C and D, the shapes of PSC/ICG@ and PSC/ICG@+DOX were nearly spherical by TEM observation. And some little particles were observed in the core of nanoparticles. The zeta potentials of PSC/ICG@ and PSC/ICG@+DOX nanoparticles were −25.21 and −20.76 mv, respectively. It was possible due to the shell of PSC with negative zeta potentials. Therefore, the hybrid PSC/ICG@+DOX nanoparticles were successfully prepared.

Photothermal Performance and Stability

The photothermal effects of ICG formulations were evaluated by a NIR laser (808 nm). As presented in Figure 3A, the temperature of ICG-containing solutions obviously increased. The increased temperature of ICG-based formulations exhibited a time-dependent manner. After laser irradiation for 5 min, the temperature of ICG solution increased by approximately 14.8°C, while the temperature values of ICG@, PSC/ICG@ and PSC/ICG@+DOX increased by 14.4°C, 12.6°C and 12.5°C, respectively. Among the groups of free ICG, ICG@, PSC/ICG@, and PSC/ICG@+DOX nanoparticles, the increased temperature was not significantly different ($P > 0.05$). The result indicated that the PSC polymeric nanoparticles and

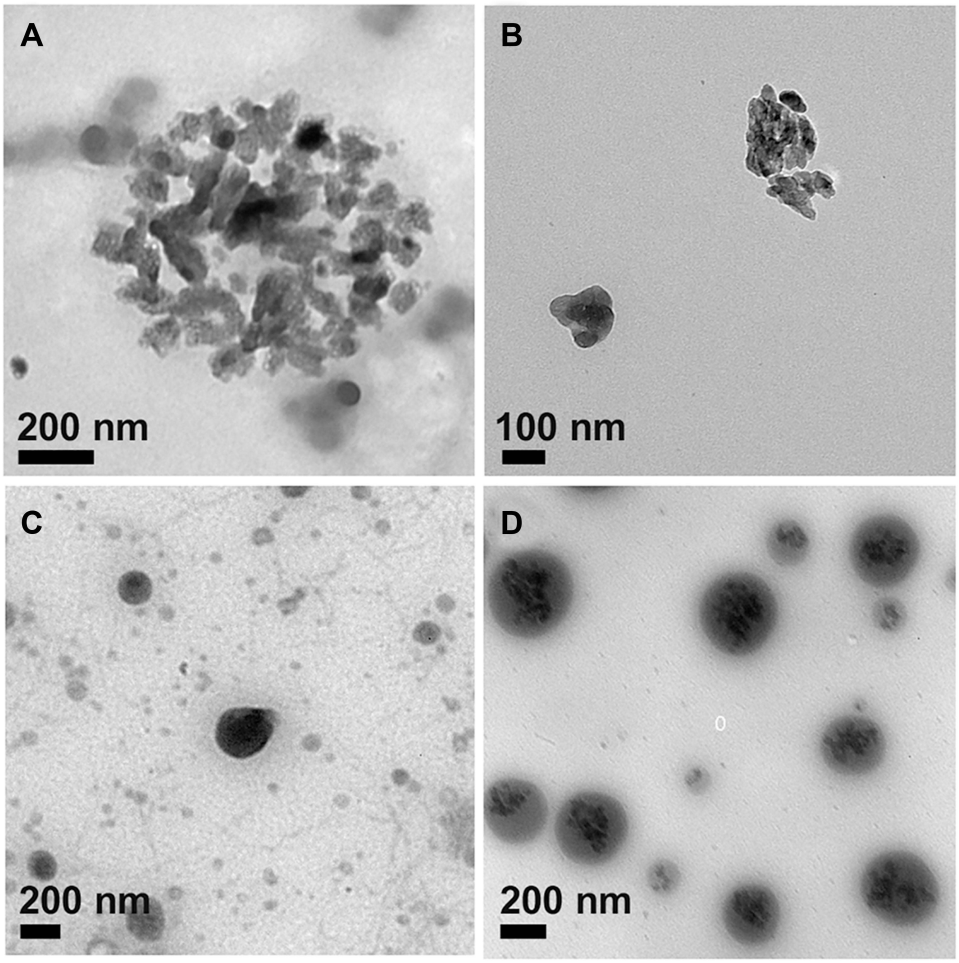

Figure 2 TEM images of (**A**) ACC, (**B**) ICG@, (**C**) PSC/ICG@ and (**D**) PSC/ICG@+DOX nanoparticles.

$CaCO_3$ nanoparticles could maintain ICG photothermal effect. In addition, PSC/ICG@ and PSC/ICG@+DOX nanoparticles exhibited slightly low temperatures than free ICG. This is due to the fact that the nanoparticles encapsulated ICG and a specific inner structure was formed through non-covalent bonds, such as hydrophobic interaction, π-π stacking force, and van der Waals force. The increased temperature of distilled water was less than 2°C. The PSC had no thermal effect. As shown in Figure 3B, the NIR thermal images exhibited temperature changes in different samples. Therefore, it inferred that the nanoparticles could shield ICG and enhance its stability. ICG-containing nanoparticles exhibited an ideal photothermal effect.

As previously described, ICG was not stable in aqueous media.[26] PSC/ICG@ and PSC/ICG@+DOX possessed 87.3% and 86.4% of absorption values after 72 h at room temperature (Figure 3C). However, free ICG was only 18.6% of its initial value at 72 h. These results demonstrated that the ICG stability was obviously improved after the protection of ACC and PSC nanoparticles. There, ICG was effectively protected from the aqueous medium by the nanoparticles.

Table 1 Physicochemical Properties of Drug-Free and Drug-Loaded Nanoparticles

Sample	Size (nm)[a]	PDI[b]	Zeta Potential (mv)	LC (%)[c]	LC (%)[d]
ACC	123±10.4	0.189±0.01	20.99±1.02	–	–
ICG@	221±12.8	0.102±0.02	30.34±1.52	12.43±0.95	–
PSC/ICG@	335±29.1	0.245±0.05	−25.21±0.66	6.39±0.84	–
PSC/ICG@+DOX	407±29.5	0.235±0.09	−20.76±0.65	2.57±0.41	6.79±0.38

Notes: [a]Measured by dynamic light scattering. [b]Polydispersity index. [c]Loading content of ICG. [d]Loading content of DOX. The results represent the mean ± SD (n=3).

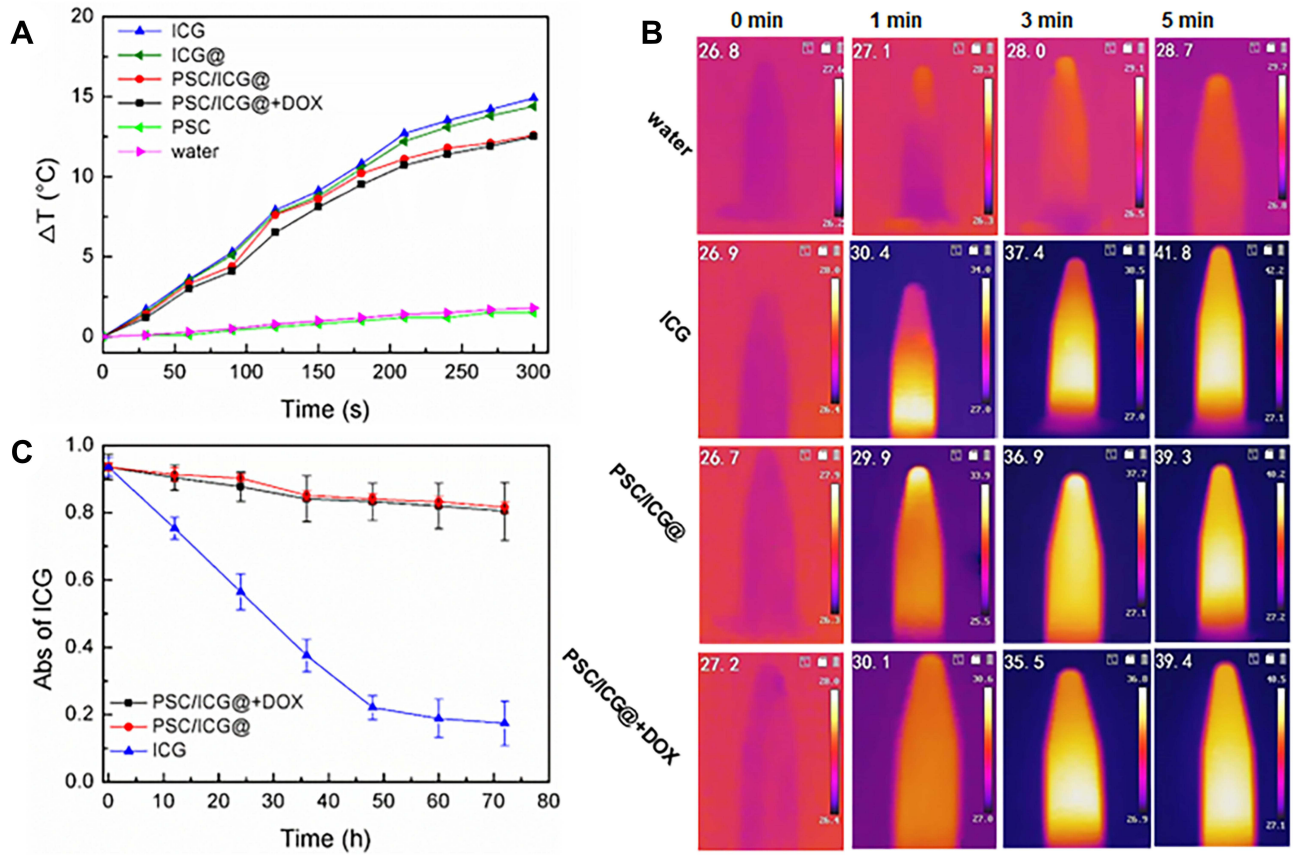

Figure 3 (**A**) Temperature changes of different formulations with the same ICG concentration (10 μg/mL) under NIR irradiation for 5 min. The temperature was determined by a thermocouple. (**B**) Infrared thermal images of water, ICG, PSC/ICG@ and PSC/ICG@+DOX nanoparticles under NIR irradiation for 5 min. (**C**) changes in absorption values of free ICG, PSC/ICG@ and PSC/ICG@+DOX nanoparticles in distilled water at 784 nm (n = 3).

In vitro Drug Release

The release profiles of PSC/ICG@+DOX nanoparticles were investigated under a simulated body environment (pH 7.4 or pH 5.5, with or without 20 mM GSH). As shown in Figure 4, the DOX cumulative rate of the nanoparticles was 29.6% at PBS (pH 7.4) up to 96 h, which was less than that (43.8%) in pH 5.5. The increased release might be ascribed to the pH-dependent decomposition of ACC and CO_2 gas production, leading to the driving force. Notably, the total release rate from PSC/ICG@

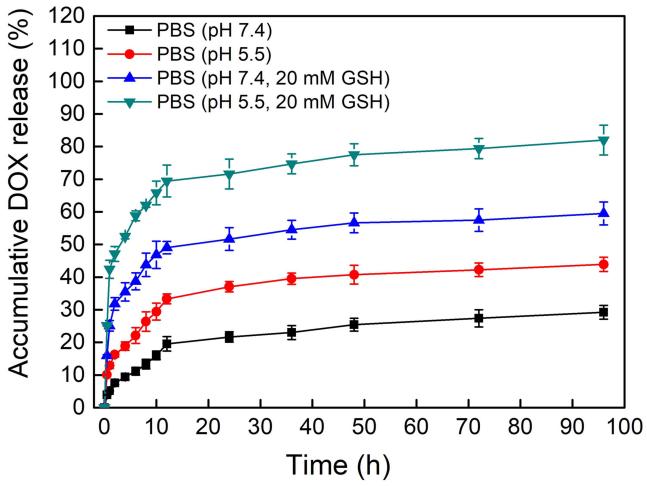

Figure 4 DOX release profiles of PSC/ICG@+DOX nanoparticles in PBS (pH 7.4, or pH 5.5) in the presence or absence of 20 mM GSH at 37°C.

+DOX nanoparticles was 82.3% in PBS (pH 5.5, 20 mM GSH), which was more than the released amount of 59.5% in PBS (pH 7.4, 20 mM GSH). Comparatively, DOX released faster from the nanoparticles under a reduction environment than that under non-reduction conditions. As previously reported, DOX-containing PSC nanoparticles showed reduction-sensitive DOX release.[19] Hence, it inferred that PSC/ICG@+DOX exhibited the dually pH/reduction-responsive characteristics. The distinctive drug release properties of the nanoparticles were expected to improve the drug bioavailability.

In vitro Cellular Uptake

The intracellular location of DOX·HCl or PSC/ICG@+DOX was investigated in 4T1 cells. As presented in Figure 5, DOX emitted red fluorescence, and Hoechst 33342 probe for nucleus staining exhibited blue fluorescence. DOX·HCl and

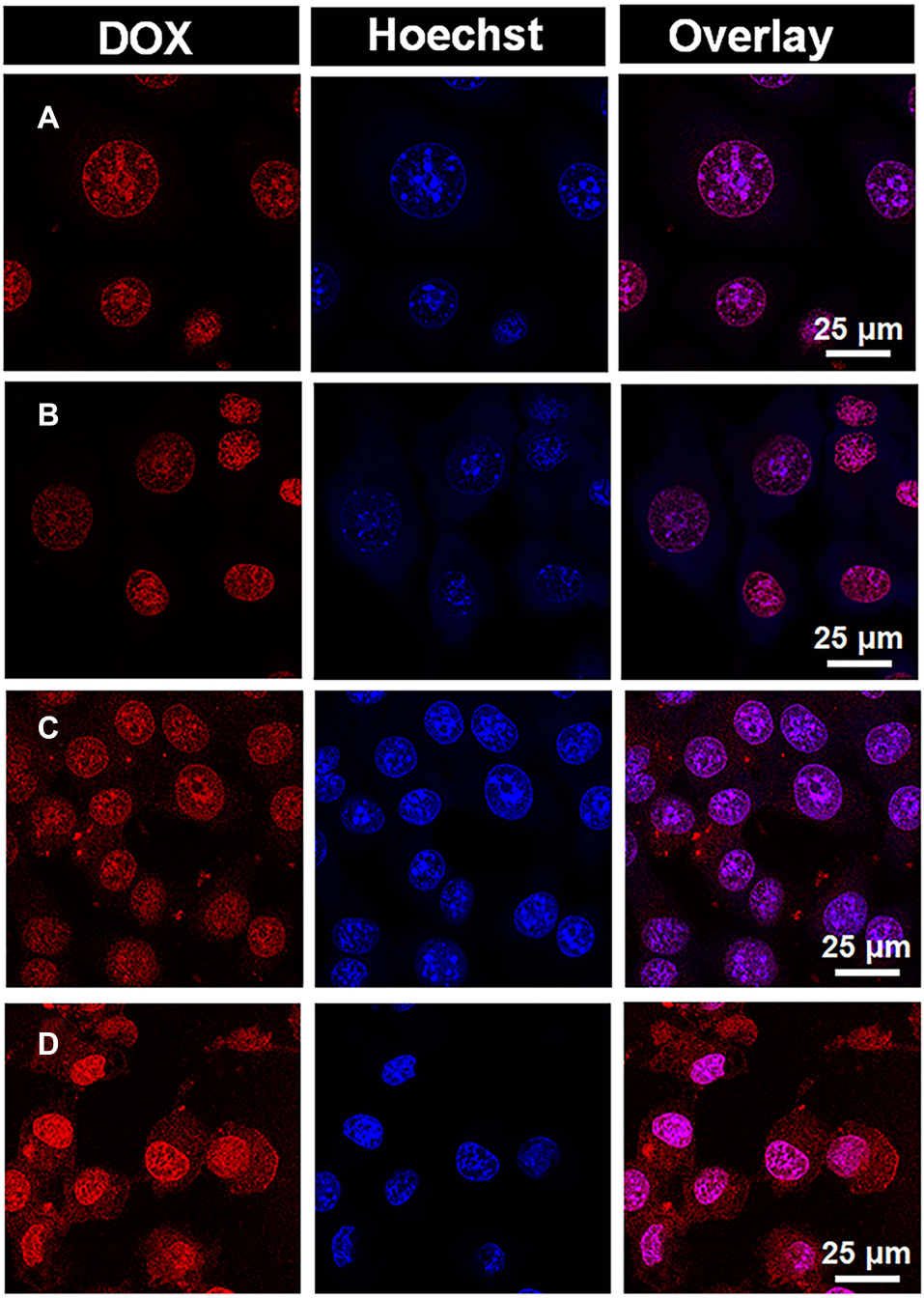

Figure 5 CLSM images of 4T1 cells treated with (**A**) DOX·HCl, (**B**) DOX·HCl+ICG (NIR), (**C**) PSC/ICG@+DOX nanoparticles (no NIR), and (**D**) PSC/ICG@+DOX nanoparticles (NIR).

DOX·HCl+ICG (NIR) were mostly located in the nucleus, and their red fluorescence exhibited similarly strong intensity. It indicated that fluorescence intensity from DOX·HCl was not changed by the addition of laser irradiation for ICG photothermal effects. Interestingly, the red fluorescence from PSC/ICG@+DOX could be seen in the cytoplasm and mainly in the nucleus. Additionally, PSC/ICG@+DOX (NIR) exhibited the strongest red fluorescence among the DOX formulations. PSC/ICG@+DOX (no NIR) showed higher fluorescence intensities than DOX·HCl and DOX·HCl+ICG (NIR). This result is ascribed to the improved uptake by CD44 receptor-mediated endocytosis and accelerated DOX release from PSC/ICG@+DOX. As stated above, the nanoparticles exhibited the pH/GSH sensitive drug release under the tumor microenvironment. Furthermore, under laser irradiation, PSC/ICG@+DOX could be rapidly dissociated and resulted in a fast release of their payloads. This finding evidenced that PSC/ICG@+DOX@ had the effects of chemotherapy and PTT.

In vitro Cytotoxicity

The cytotoxicity was investigated in 4T1 cells by the MTT assay. To study the activity of chemo-PTT mediated PSC/ICG@+DOX nanoparticles, other groups were conducted which included free ICG, DOX·HCl, DOX·HCl+ICG, PSC/ICG@, PSC/ICG@+DOX. As shown in Figure 6A, without laser irradiation, all groups exhibited concentration-dependent cell inhibition. PSC/ICG@+DOX showed the strongest killing activity against 4T1 cells. It agreed with the results of CLSM observations. PSC/ICG@+DOX nanoparticles could enhance cellular uptake and exhibit intelligent DOX release with stimuli responsiveness. DOX and DOX·HCl+ICG demonstrated similar cytotoxic effects. This indicated that ICG had a negligible effect on cell killing. Compared with these above groups, PSC/ICG@ displayed the lowest cell inhibition (less than 15%) at the same concentrations. This result might be ascribed to the production of disruptive force and CO_2 bubbles from $CaCO_3$ nanoparticles under an acid environment.[35]

As displayed in Figure 6B, with NIR irradiation, the cell inhibition also was concentration dependent in these groups. The order of the cytotoxic activities among these groups was followed as: PSC/ICG@+DOX (NIR) > DOX·HCl+ICG (NIR) >PSC/ICG@ (NIR) > ICG (NIR). At the same concentration, PSC/ICG@+DOX, DOX·HCl+ICG and PSC/ICG@ exhibited the increased inhibition after NIR irradiation. These phenomena revealed the synergistic effect of PTT-chemotherapy in 4T1 cells. It also coincided with CLSM studies. Additionally, free ICG with laser irradiation showed toxic activity against 4T1 cells. Moreover, drug-free PSC nanoparticles were not cytotoxic in 4T1 cells at the equivalent polymer concentration of PSC/ICG@+DOX in the presence or absence of the NIR laser (data not shown). We inferred that PSC/ICG@+DOX would effectively deliver the drug into the tumor in vivo.

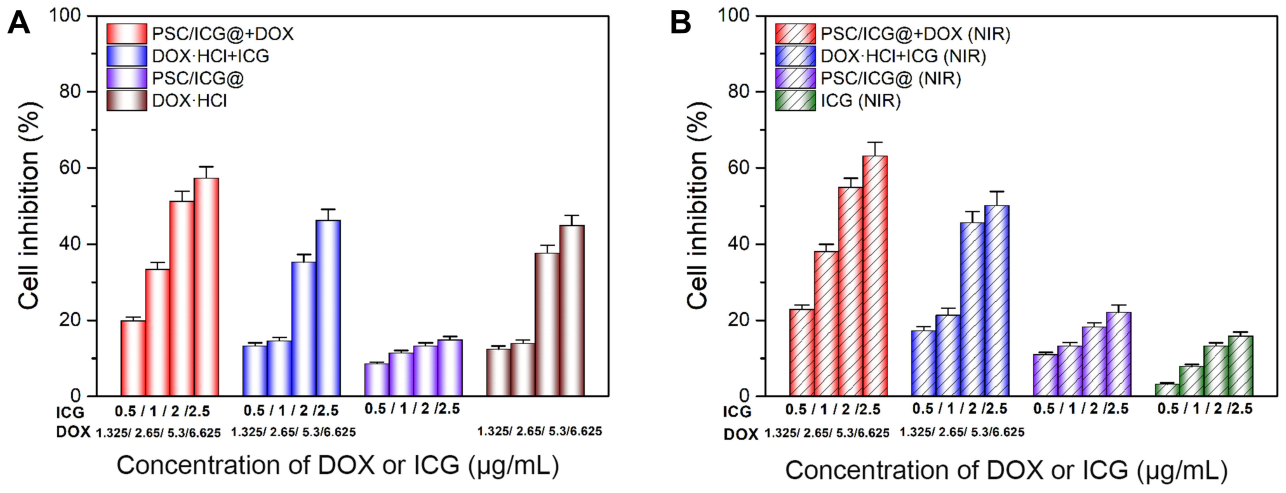

Figure 6 In vitro cytotoxicity in 4T1 cells treated with DOX·HCl, ICG, DOX·HCl+ICG, PSC/ICG@ nanoparticles, PSC/ICG@+DOX nanoparticles in the absence (**A**) or presence (**B**) of 808 nm NIR irradiation. (n=4).

Biocompatibility Preliminary Evaluation

To investigate the biocompatibility of nanoparticles, the hematological levels of RBC, WBC and platelet counts were measured. As presented in Figure S2 (Supporting Information), no significant differences were observed in all parameters for these nanoparticle groups compared with 5% glucose group ($P > 0.05$). Additionally, the liver function markers (total bilirubin, AST, ALT) and kidney function indicators (BUN, creatinine levels) were also detected. The biochemical levels were in the normal range among all groups (Figure S2). Furthermore, the body weight increased in all groups (Figure S3, Supporting Information). These results convincingly confirmed that our designed nanoparticles had good biosafety for antitumor application in vivo.

In vivo Antitumor Effects

Encouraged by the high cellular uptake and cytotoxicity of PSC/ICG@+DOX in vitro, we further investigated the chemo-PTT efficacy in 4T1 tumor-bearing orthotopic mice model. The change rate of tumor volume, which was relative to the start point, is shown in Figure 7. Both 5% glucose and PSC groups showed almost similar phenomena with rapid tumor growth during the experiment. Free ICG (NIR) exhibited slight suppression compared with 5% glucose group ($P > 0.05$). PSC/ICG@ nanoparticles demonstrated more inhibition of tumor growth than ICG (NIR) group. This is partly due to the decomposition

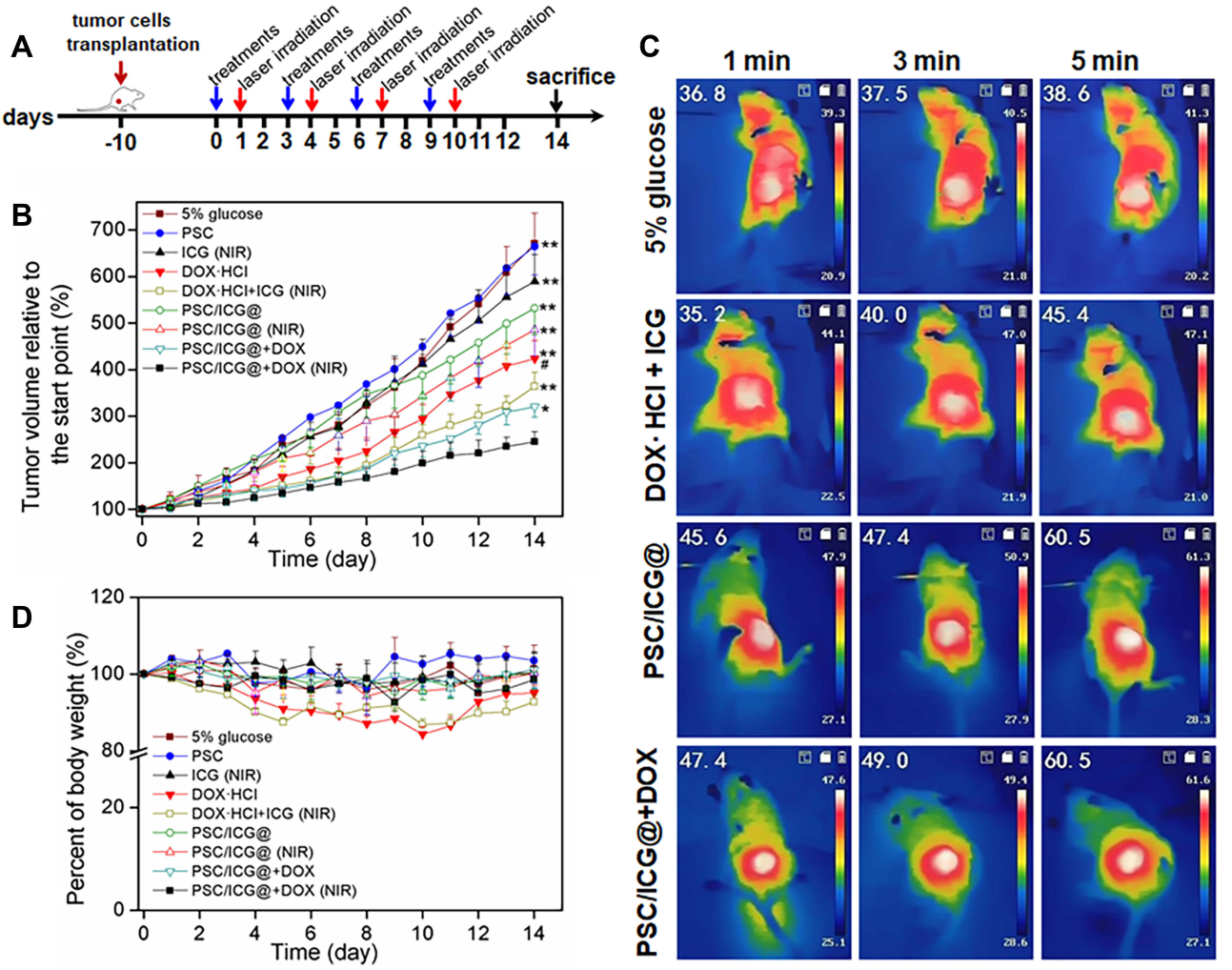

Figure 7 (**A**) Scheme of the timeline for in vivo treatment and laser irradiation in 4T1-bearing orthotopic mice. (**B**) Tumor growth curves of mice after the treatment. (**C**) The images of 4T1-bearing mice with the injection of 5% glucose, DOX·HCl+ICG, PSC/ICG@ or PSC/ICG@+DOX nanoparticle after laser irradiation under the 808 nm laser irradiation (2.0 W/cm^2) at 24 h post-injection. (**D**) Body weight change within 14 days. *$P < 0.05$, PSC/ICG@+DOX (NIR) group vs PSC/ICG@+DOX (no NIR) group; **$P < 0.01$ PSC/ICG@+DOX (NIR) group vs other groups; $^{\#}P < 0.05$, PSC/ICG@+DOX group (no NIR) vs DOX·HCl group. (n=5).

of calcium carbonate and the generation of CO_2 bubbles under acid microenvironment,[1] and the efficient retention of the nanoparticles by the EPR effect.[36,37] The thermal images of tumor sites are shown in Figure 7C. The tumor temperature in 5% glucose group was slightly increased after 5 min of laser irradiation. Free DOX+ICG (NIR) group exhibited the tumor temperature with an increase to 45.4°C. Notably, PSC/ICG@ and PSC/ICG@+DOX groups showed an increased temperature of 60.5°C after 5 min irradiation, which could effectively generate hyperthermia for PTT of malignant tumors.[38] Free DOX·HCl showed moderately delayed growth. PSC/ICG@+DOX (no NIR) revealed stronger tumor suppression in contrast with DOX·HCl group. As previously reported,[39,40] polymeric nanoparticles could prolong blood circulation in vivo. Further, chondroitin sulfate and its derivatives were employed for targeting drug delivery on the CD44-overexpressed surface of cancer cells.[41–44] Therefore, PSC/ICG@+DOX nanoparticles could actively transport into CD44 receptor-positive 4T1 tumors. The pH/reduction-sensitive drug release from the nanoparticles could increase the concentration of drug molecules at the targeted tumor sites. Importantly, the tumor growth in mice treated by PSC/ICG@+DOX (NIR) group was the strongest inhibition among these groups, which was significantly different with PSC/ICG@+DOX (no NIR) ($P < 0.05$), and very significant with ICG +DOX group (plus NIR) ($P < 0.01$). It was due to the combined photothermal and chemotherapy. Hence, the result demonstrated the superior synergistic antitumor effects of PSC/ICG@+DOX nanoparticles. As presented in Figure 7D, both DOX·HCl and DOX·HCl+ICG groups showed body weight loss on some days. It inferred that free DOX molecule was distributed into normal cells, leading to side effects in tumor-bearing mice.[45] The average body weights in other groups showed no obvious decrease. These results demonstrated that DOX-loaded nanoparticles could increase DOX gathering in the tumor sites and avoid undesirable toxicities.

To further assess the antitumor activities in all treatments, HE and TUNEL assays were performed. As shown in Figure 8, HE images exhibited that larger degrees of cell morphological change and necrosis were observed in the tumor issue of PSC/ICG@+DOX (NIR) group in comparison to other groups. It also revealed the synergistic chemotherapy and PTT effects. To further investigate the cell apoptosis in tumor tissues, TUNEL analysis was applied. As displayed in Figure S4 (Supporting

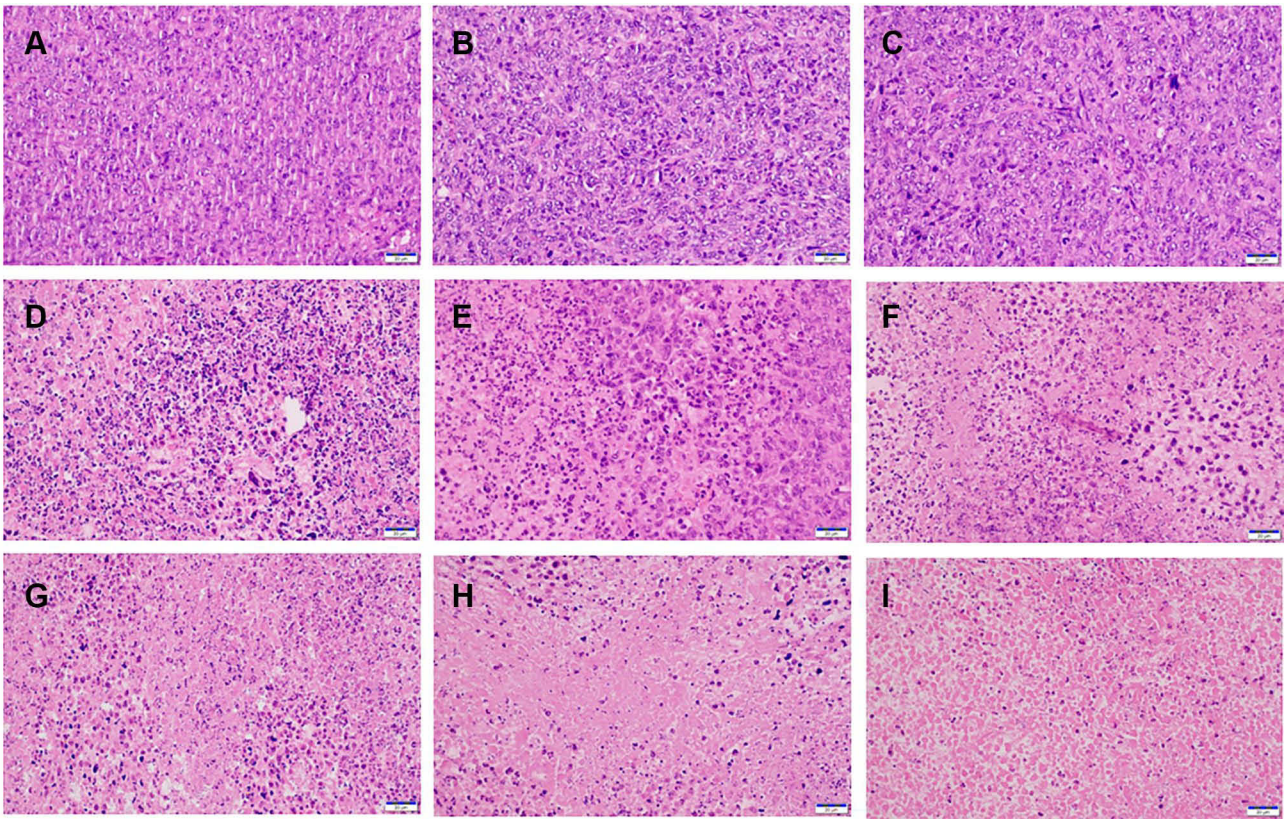

Figure 8 H&E staining images of the tumors with the treatments of (**A**) 5% glucose, (**B**) PSC, (**C**) ICG (NIR), (**D**) PSC/ICG@, (**E**) PSC/ICG@ (NIR), (**F**) DOX·HCl, (**G**) DOX·HCl+ICG (NIR), (**H**) PSC/ICG@+DOX, and (**I**) PSC/ICG@+DOX (NIR), respectively. Scale bar, 20 μm.

Information), the number of apoptotic cells in PSC/ICG@+DOX (NIR) group was more than those of other groups. It agreed with the result of tumor growth inhibition in vivo. The expression of Ki67 protein was further determined to the inhibition of proliferation in the tumors. In Figure S5 (Supporting Information), PSC/ICG@+DOX (NIR) group demonstrated the lowest expression of Ki67 among all groups. These results were in accordance with the tumor volume changes in the treatment groups. Therefore, the histological analysis evidenced the combined and effective therapeutic efficacy of PSC/ICG@+DOX nanoparticles.

Conclusions

In summary, a new class of tumor-targeted and dual stimuli-responsive nanoplatforms based on PSC-encapsulating ICG@ and DOX was successfully developed. The hybrid nanoparticles were evaluated for efficient loading of different types of chemotherapeutic and photothermal molecules. Our PSC/ICG@+DOX nanoparticles would be degraded and increased drug release under a slightly acidic solution and reduction environment. Additionally, PSC/ICG@+DOX exhibited an efficient photothermal effect in vitro, and enhanced cellular uptake and cytotoxicity in 4T1 cells. Importantly, the multifunctional drug-loaded nanoparticles demonstrated superior synergistic antitumor effects in 4T1-bearing mice, and the combined photothermal and chemotherapy were revealed. Therefore, this work presents that the tumor-pH-activated, reduction-sensitive, and actively targeted nanocarrier could be effectively used in future cancer treatment.

Supporting Information

The DSC thermograms of PSC/ICG@ and PSC/ICG@+DOX nanoparticles, body weight changes, blood routine and biochemistry analysis, TUNEL and Ki67 staining of the tumors were presented in the Supporting Information (Figures S1–S5).

Acknowledgments

This work was funded by the Natural Science Foundation of Jiangxi Province (20202BABL206155 and 20192ACBL20032), Scientific Research Fund of Education Department of Jiangxi Province (GJJ201820), and Scientific Research Fund of Health Commission of Jiangxi Province (202211975).

Disclosure

The authors report no conflicts of interest in this work.

References

1. Wang C, Chen SQ, Yu Q, et al. Taking advantage of the disadvantage: employing the high aqueous instability of amorphous calcium carbonate to realize burst drug release within cancer cells. *J Mater Chem B*. 2017;5:2068–2073. doi:10.1039/C6TB02826H
2. Zhao Y, Luo Z, Li MH, et al. A preloaded amorphous calcium carbonate/doxorubicin@silica nanoreactor for ph-responsive delivery of an anticancer drug. *Angewandte Chemie*. 2015;54:919–922. doi:10.1002/anie.201408510
3. Xue -C-C, Li M-H, Zhao Y, et al. Tumor microenvironment-activatable fe-doxorubicin preloaded amorphous $CaCO_3$ nanoformulation triggers ferroptosis in target tumor cells. *Sci Adv*. 2020;6:eaax1346. doi:10.1126/sciadv.aax1346
4. Chen S-F, Coelfen H, Antonietti M, et al. Ethanol assisted synthesis of pure and stable amorphous calcium carbonate nanoparticles. *Chem Commun*. 2013;49:9564–9566. doi:10.1039/c3cc45427d
5. Wang C, Yu F, Liu X, et al. Cancer-specific therapy by artificial modulation of intracellular calcium concentration. *Adv Healthcare Mater*. 2019;8:1900501. doi:10.1002/adhm.201900501
6. Tan M, Liu W, Liu F, et al. Silk fibroin-coated nanoagents for acidic lysosome targeting by a functional preservation strategy in cancer chemotherapy. *Theranostics*. 2019;9:961–973.
7. Wang C, Liu X, Chen S, et al. Facile preparation of phospholipid-amorphous calcium carbonate hybrid nanoparticles: toward controllable burst drug release and enhanced tumor penetration. *Chem Commun*. 2018;54:13080–13083. doi:10.1039/C8CC07694D
8. Liu X, Wang C, Ma H, et al. Water-responsive hybrid nanoparticles codelivering ICG and DOX effectively treat breast cancer via hyperthermia-aided DOX functionality and drug penetration. *Adv Healthcare Mater*. 2019;8:1801486.
9. Park J, Jo S, Lee YM, et al. Enzyme-triggered disassembly of polymeric micelles by controlled depolymerization via cascade cyclization for anticancer drug delivery. *ACS Appl Mater Interfaces*. 2021;13:8060–8070.
10. Feng X, Zhou Y, Xie X, et al. Development of PSMA-targeted and core-crosslinked glycol chitosan micelles for docetaxel delivery in prostate cancer therapy. *Mater Sci Eng C*. 2019;96:436–445. doi:10.1016/j.msec.2018.11.044
11. Kaur J, Mishra V, Singh SK, et al. Harnessing amphiphilic polymeric micelles for diagnostic and therapeutic applications: breakthroughs and bottlenecks. *J Control Release*. 2021;334:64–95. doi:10.1016/j.jconrel.2021.04.014
12. Hao Y, Gao Y, Fan Y, et al. A tumor microenvironment-responsive poly(amidoamine) dendrimer nanoplatform for hypoxia-responsive chemo/chemodynamic therapy. *J Nanobiotechnology*. 2022;20:43. doi:10.1186/s12951-022-01247-6

13. Song CF, Lin TT, Zhang Q, et al. Ph-sensitive morphological transitions in polymeric tadpole assemblies for programmed tumor therapy. *J Control Release*. 2019;293:1–9. doi:10.1016/j.jconrel.2018.10.033
14. Chen W, Zou Y, Zhong Z, et al. Cyclo(RGD)-decorated reduction-responsive nanogels mediate targeted chemotherapy of integrin overexpressing human glioblastoma in vivo. *Small*. 2017;13:1601997. doi:10.1002/smll.201601997
15. Liu H, Wu S, Yu J, et al. Reduction-sensitive micelles self-assembled from amphiphilic chondroitin sulfate A-deoxycholic acid conjugate for triggered release of doxorubicin. *Mater Sci Eng C*. 2017;75:55–63. doi:10.1016/j.msec.2017.02.030
16. Gu W, Liu T, Fan D, et al. A6 peptide-tagged, ultra-small and reduction-sensitive polymersomal vincristine sulfate as a smart and specific treatment for CD44+acute myeloid leukemia. *J Control Release*. 2021;329:706–716. doi:10.1016/j.jconrel.2020.10.005
17. Du J, Zong L, Li M, et al. Two-pronged anti-tumor therapy by a new polymer-paclitaxel conjugate micelle with an anti-multidrug resistance effect. *Int J Nanomedicine*. 2022;17:1323–1341. doi:10.2147/IJN.S348598
18. Ma ZC, Wu JP, Sun MC, et al. Disulfur-bridged polyethyleneglycol/DOX nanoparticles for the encapsulation of photosensitive drugs: a case of computational simulations on the redox-responsive chemo-photodynamic drug delivery system. *RSC Adv*. 2021;11:37988–37994. doi:10.1039/D1RA05645J
19. Wang X-F, Ren J, He H-Q, et al. Self-assembled nanoparticles of reduction-sensitive poly (lactic-co-glycolic acid)-conjugated chondroitin sulfate a for doxorubicin delivery: preparation, characterization and evaluation. *Pharm Dev Technol*. 2019;24:794–802. doi:10.1080/10837450.2019.1599914
20. Liang CH, Bai XY, Qi CL, et al. Pi electron-stabilized polymeric micelles potentiate docetaxel therapy in advanced-stage gastrointestinal cancer. *Biomaterials*. 2021;266:120432. doi:10.1016/j.biomaterials.2020.120432
21. Krishnan N, Fang RNH, Zhang LF. Engineering of stimuli-responsive self-assembled biomimetic nanoparticles. *Adv Drug Deliv Rev*. 2021;179:114006. doi:10.1016/j.addr.2021.114006
22. Wei G, Wang Y, Yang G, et al. Recent progress in nanomedicine for enhanced cancer chemotherapy. *Theranostics*. 2021;11:6370–6392. doi:10.7150/thno.57828
23. Cheng H, Jiang ZJ, Sun CK, et al. Protein stabilized polymeric nanoparticles inspired relay drug delivery for tackling post-chemotherapeutic metastasis. *Chem Eng J*. 2022;427:131672. doi:10.1016/j.cej.2021.131672
24. Cheng X, He L, Xu J, et al. Oxygen-producing catalase-based prodrug nanoparticles overcoming resistance in hypoxia-mediated chemo-photodynamic therapy. *Acta Biomaterialia*. 2020;112:234–249. doi:10.1016/j.actbio.2020.05.035
25. Zhu XJ, Feng W, Chang J, et al. Temperature-feedback upconversion nanocomposite for accurate photothermal therapy at facile temperature. *Nat Commun*. 2016;7:10437. doi:10.1038/ncomms10437
26. Ma Y, Tong S, Bao G, et al. Indocyanine green loaded SPIO nanoparticles with phospholipid-peg coating for dual-modal imaging and photothermal therapy. *Biomaterials*. 2013;34:7706–7714. doi:10.1016/j.biomaterials.2013.07.007
27. Ogawa M, Kosaka N, Choyke PL, et al. In vivo molecular imaging of cancer with a quenching near-infrared fluorescent probe using conjugates of monoclonal antibodies and indocyanine green. *Cancer Res*. 2009;69:1268–1272. doi:10.1158/0008-5472.CAN-08-3116
28. Li Y, Yang L, Xu X, et al. Multifunctional size-expandable nanomedicines enhance tumor accumulation and penetration for synergistic chemo-photothermal therapy. *ACS Appl Mater Interfaces*. 2021;13:46361–46374. doi:10.1021/acsami.1c14170
29. Yang L, Hou X, Zhang Y, et al. NIR-activated self-sensitized polymeric micelles for enhanced cancer chemo-photothermal therapy. *J Control Release*. 2021;339:114–129. doi:10.1016/j.jconrel.2021.09.017
30. Zhu AJ, Miao K, Deng YB, et al. Dually pH/reduction-responsive vesicles for ultrahigh-contrast fluorescence imaging and thermo-chemotherapy-synergized tumor ablation. *ACS Nano*. 2015;9:7874–7885. doi:10.1021/acsnano.5b02843
31. Cai S, Xie X, Yuan Q, et al. Preparation and evaluation of reduction-responsive micelles based on disulfide-linked chondroitin sulfate A-tocopherol succinate for controlled antitumour drug release. *J Pharm Pharmacol*. 2021;73:1405–1417. doi:10.1093/jpp/rgab096
32. Yu J, Xie X, Xu X, et al. Development of dual ligand-targeted polymeric micelles as drug carriers for cancer therapy in vitro and in vivo. *J Mater Chem B*. 2014;2:2114–2126. doi:10.1039/c3tb21539c
33. Yin T, Chu X, Cheng J, et al. Hypoxia-sensitive zwitterionic vehicle for tumor-specific drug delivery through antifouling-based stable biotransport alongside PDT-sensitized controlled release. *Biomacromolecules*. 2021;22:2233–2247. doi:10.1021/acs.biomac.1c00301
34. Dizaj SM, Lotfipour F, Barzegar-Jalali M, et al. Physicochemical characterization and antimicrobial evaluation of gentamicin-loaded $CaCO_3$ nanoparticles prepared via microemulsion method. *J Drug Deliv Sci Technol*. 2016;35:16–23. doi:10.1016/j.jddst.2016.05.004
35. Chung M-F, Chen K-J, Liang H-F, et al. A liposomal system capable of generating CO_2 bubbles to induce transient cavitation, lysosomal rupturing, and cell necrosis. *Angewandte Chemie*. 2012;51:10089–10093. doi:10.1002/anie.201205482
36. Mirhadi E, Mashreghi M, Maleki MF, et al. Redox-sensitive nanoscale drug delivery systems for cancer treatment. *Int J Pharm*. 2020;589:119882. doi:10.1016/j.ijpharm.2020.119882
37. Jeon S, Jun E, Chang H, et al. Prediction the clinical epr effect of nanoparticles in patient-derived xenograft models. *J Control Release*. 2022;351:37–49. doi:10.1016/j.jconrel.2022.09.007
38. Yang Y, Yun K, Li Y, et al. Self-assembled multifunctional polymeric micelles for tumor-specific bioimaging and synergistic chemo-phototherapy of cancer. *Int J Pharm*. 2021;602:120651. doi:10.1016/j.ijpharm.2021.120651
39. Long M, Liu X, Huang X, et al. Alendronate-functionalized hypoxia-responsive polymeric micelles for targeted therapy of bone metastatic prostate cancer. *J Control Release*. 2021;334:303–317. doi:10.1016/j.jconrel.2021.04.035
40. Zhou H, Fan Z, Li PY, et al. Dense and dynamic polyethylene glycol shells cloak nanoparticles from uptake by liver endothelial cells for long blood circulation. *ACS Nano*. 2018;12:10130–10141. doi:10.1021/acsnano.8b04947
41. Lee J-Y, Chung S-J, Cho H-J, et al. Phenylboronic acid-decorated chondroitin sulfate A-based theranostic nanoparticles for enhanced tumor targeting and penetration. *Adv Funct Mater*. 2015;25:3705–3717. doi:10.1002/adfm.201500680
42. Yu C, Gao C, Lu S, et al. Facile preparation of pH-sensitive micelles self-assembled from amphiphilic chondroitin sulfate-histamine conjugate for triggered intracellular drug release. *Colloids Surf B Biointerfaces*. 2014;115:331–339. doi:10.1016/j.colsurfb.2013.12.023
43. Yu C, Gao C, Lu S, et al. Redox-responsive shell-sheddable micelles self-assembled from amphiphilic chondroitin sulfate-cholesterol conjugates for triggered intracellular drug release. *Chem Eng J*. 2013;228:290–299. doi:10.1016/j.cej.2013.04.083
44. Li H, Zhang P, Luo J, et al. Chondroitin sulfate-linked prodrug nanoparticles target the Golgi apparatus for cancer metastasis treatment. *ACS Nano*. 2019;13:9386–9396. doi:10.1021/acsnano.9b04166
45. Han K, Zhang W-Y, Zhang J, et al. pH-responsive nanoscale coordination polymer for efficient drug delivery and real-time release monitoring. *Adv Healthcare Mater*. 2017;6:1700470. doi:10.1002/adhm.201700470